

Surface Functions during Mitosis. III. Quantitative Analysis of Ligand-receptor Movement into the Cleavage Furrow: Diffusion vs. Flow

D. E. KOPPEL, J. M. OLIVER, and R. D. BERLIN

Departments of Biochemistry and Physiology, University of Connecticut Health Center, Farmington, Connecticut 06032

ABSTRACT The surface distribution of concanavalin A (Con A) bound to cell membrane receptors varies dramatically as a function of mitotic phase. The lectin is distributed diffusely on cells labeled and observed between mid-prophase and early anaphase, whereas cells observed in late anaphase or telophase demonstrate a marked accumulation of Con A-receptor complexes over the developing cleavage furrow (Berlin, Oliver, and Walter. 1978. *Cell*. 15:327-341). In this report, we first use a system based on video intensification fluorescence microscopy to describe the simultaneous changes in cell shape and in lectin-receptor complex topography during progression of single cells through the mitotic cycle. The video analysis establishes that fluorescein succinyl Con A (F-S Con A)-receptor complex redistribution begins coincident with the first appearance of the cleavage furrow and is essentially complete within 2-3 min. This remarkable redistribution of surface fluorescence occurs during only a modest change in cell shape from a sphere to a belted cylinder. It reflects the translocation of complexes and not the accumulation of excess labeled membrane in the cleavage furrow: first, bound fluorescent cholera toxin which faithfully outlines the plasma membrane is not accumulated in the cleavage furrow, and, second, electron microscopy of peroxidase-Con A labeled cells undergoing cleavage shows that there is a high linear density of lectin within the furrow while Con A is virtually eliminated from the poles. The rate of surface movement of F-S Con A was quantitated by photon counting during a repetitive series of laser-excited fluorescence scans across dividing cells. Results were analyzed in terms of two alternative models of movement: a flow model in which complexes moved unidirectionally at constant velocity, and a diffusion model in which complexes could diffuse freely but were trapped at the cleavage furrow. According to these models, the observed rates of accumulation were attainable at either an effective flow velocity of $\sim 1 \mu\text{m}/\text{min}$, or an effective diffusion coefficient of $\sim 10^{-9} \text{ cm}^2/\text{s}$. However, in separate experiments the lectin-receptor diffusion rate measured directly by the method of fluorescence recovery after photobleaching (FRAP) on metaphase cells was only $\sim 10^{-10} \text{ cm}^2/\text{s}$. Most importantly, photobleaching experiments during the actual period of F-S Con A accumulation showed that lectin-receptor movement during cleavage occurs unidirectionally. These results rule out diffusion and make a process of oriented flow of ligand-receptor complexes the most likely mechanism for ligand-receptor accumulation in the cleavage furrow.

The distribution of surface-bound concanavalin A (Con A) varies dramatically with mitotic phase, remaining diffuse from prophase through metaphase and then showing a striking accumulation in the cleavage furrow at anaphase and telophase (2). The movement of Con A-receptor complexes into the

cleavage furrow appears analogous to their movement into the pseudopods of phagocytic cells, the uropods of oriented cells, or into the protuberance of cells forming caps (1, 24). The array of hypotheses developed to explain the movement of lectin-receptor and antibody-receptor complexes (eg., refer-

ences 5, 6, 9, 10, 13, 14, 26) may be divided into two broad groups. In the first, some active "contractile" apparatus is supposed either to interact directly with the ligand-receptor complex or to cause wave motion and the entrainment of complexes. In the second, the diffusion of the ligand-receptor complex and its progressive cross-linking into large aggregates is thought to be fundamental. Combinations of elements of these two groups are also possible. The strengths and weaknesses of these various proposals were recently evaluated (24). However, the physical characterization of the movement has not been made in such a way as to establish one particular mechanism.

The movement of ligand-receptor complexes into the cleavage furrow seems particularly favorable for this analysis. First, the cell geometry and direction of receptor movement is simple and predictable (perpendicular to the metaphase plate). This allows convenient positioning of the cell for measurement and simplifies analysis of the data. Second, pinocytosis is virtually absent during mitosis (2, 3) so that the bound ligand is confined to the surface during the entire period of measurement. This removes ambiguities arising from fluorescent signals produced by internalized ligands. It was also hoped that the analysis could shed light on the control of ligand-receptor movement during the fundamental biological process of cytokinesis.

MATERIALS AND METHODS

J774.2 mouse macrophages were kindly provided by Dr. O. Rosen and Dr. B. Bloom (Albert Einstein School of Medicine) (23). They were selected from a line originally developed by Dr. P. Ralph (Sloan-Kettering Institute) (25). The cells were grown on 13-mm diameter glass cover slips in Dulbecco's modified Eagle's medium (DME) supplemented with 20% horse serum as described before (2).

Fluorescein-conjugated Succinyl Con A Labeling

Monolayers of J774.2 cells were rinsed through four changes of phosphate-buffered saline with 2 mM MgCl₂, 1 mM CaCl₂, 5 mM glucose, and 1% bovine serum albumin (PBS-BSA). They were labeled with fluorescein-conjugated succinyl concanavalin A (F-S Con A) (Vector Laboratories, Burlingame, CA) at 50–100 µg/ml for 1–2 min at room temperature in PBS-BSA. Subsequently, the cover slips were rinsed and inverted over ~25 µl of PBS-BSA contained within a well of high vacuum grease (Dow Corning Corp., Midland, MI) on a glass slide.

Fluorescein-Cholera Toxin B Labeling

The B (binding) subunit of cholera toxin (Calbiochem-Behring Corp., San Diego, CA) was fluorescence labeled by incubation for 30 min at 4°C in phosphate-buffered saline with dichlorotriazinylaminofluorescein (DTAF-Research Organics, Cleveland, OH) and overnight dialysis to remove unbound fluorochrome. SDS PAGE of the product showed a single coincident fluorescent and Coomassie-Blue-stained band at ~10,000 daltons (21). Cell monolayers were labeled in PBS-BSA with 10 µg/ml fluorescein-cholera toxin B (F-CTB) for 10 min at 37°C. The cells were fixed for 10 min at 37°C with 4% paraformaldehyde either before or after incubation with cholera toxin.

Observation of Mitotic Cells

For the laser studies, cells in mitosis were detected by phase-contrast microscopy. For fluorescence photomicroscopy, detection of mitotic cells was simplified by incubation of monolayers for 10 min at 37°C with 2 µg/ml of the bisbenzimidazole dye Hoechst 33662 (living cells) or 1 µg/ml Hoechst 33258 (fixed cells) before mounting. These DNA-binding dyes were obtained by courtesy of Hoechst-Roussel, NJ. Hoechst 33662 penetrates living cells. Hoechst 33258 provides somewhat finer resolution than Hoechst 33662 but only penetrates living cells at high concentrations.

Fluorescence Photomicroscopy

Fluorescence-labeled cells were observed with a Zeiss Photomicroscope III equipped with a III RS epi-illuminator and 100 W mercury lamp source. Hoechst

dye and fluorescein emission spectra were optically separated with a band pass excitation filter BP 390–440 nm, with an FT 460 dichroic mirror and LP 475 barrier filter (Hoechst) and standard Zeiss filter combinations for fluorescein (2). These filter combinations allowed observation of chromosome organization and surface ligand fluorescence on the same cell. Phase contrast was observed through a green interference filter (BP 546–10). The cells were photographed on Kodak Tri-X Pan film.

Video Intensification Fluorescence Microscopy

The movement of F-S Con A over the mitotic cell surface was observed by use of low light fluorescence excitation and high resolution video intensification recording. Slides were placed on the stage of a Zeiss universal microscope equipped with the III RS epilluminator and 100 W Hg lamp. Stage temperature was set by use of a Sage air curtain incubator (Orion Research Inc., Cambridge, MA) or a Cambion temperature-controlled stage (Cambridge Thermionic Corp., Cambridge, MA). Neutral density filters were used to maintain the exciting light at or below the limit of visual observation.

The fluorescence image was obtained using a Venus DV 3 three stage intensification camera (Venus Scientific Inc., Farmingdale, NY) with vidicon tube. This camera was selected for its superior resolution at low light levels as compared to intensifiers using silicon intensified target (SIT) tubes. The image was transferred to a Quantex Digital Image Processor (Quantex Corp., Sunnyvale, CA) which digitizes each frame into a large (512 x 512 x 12 bit) memory and enables a variety of image manipulations (summation, averaging, image inversion, nonlinear operation, etc.) that greatly improve the resolution and information content of video images. Processed images were displayed on a Tektronix 634 monitor (Tektronix Inc., Beaverton, OR), selected for its high resolution and stability. The signals from individual rasters were simultaneously displayed on a Tektronix T935A oscilloscope to check stability and absence of saturation. Finally the images were recorded using an IVC 1010 1" videotape recorder with 800 line resolution (International Video Corp., Sunnyvale, CA). This recorder provides a faithful linear record of the camera signal even at extremes of light and dark.

Individual tape films were analyzed by playback into the image processor and transfer of selected frames to the monitor. Images were photographed with Polaroid 611 CRT screen film and Kodak Tri-X-Pan film using a Tektronix C-28 camera. A time generator (Thalner Electronic Laboratories, Inc., Ann Arbor, MI) between the image processor and monitor enabled accurate placement in time (seconds) of events during recording and later analysis of tapes.

For the experiment reported here, J774.2 mouse macrophages were incubated for 10 min at 37°C with Hoechst 33662, rinsed, labeled with 50 µg/ml F-S-Con A for 1 min, then placed on the microscope stage at 32°C. A cell in metaphase was selected by fluorescence microscopy using a × 63 phase/neo-fluar objective and scanning the cell population by use of the DV3 camera and monitor. The surface-bound F-S Con A of the chosen cell was illuminated with low levels of exciting light. The camera was set in the automatic gain mode, the Quantex was set in a 64-frame averaging mode which provides a running average of the video signal and reduces noise by \sqrt{N} where N = number of frames averaged (in this case by eightfold). Cells were observed to progress into anaphase, telophase, and, eventually, G₁. Photographs were taken on playback of tapes of one of several cells that traversed the mitotic cycle from metaphase into G₁.

Quantification of Ligand Distribution and Movement

For experiments employing the laser apparatus, cells were labeled at room temperature for 2 min with 100 µg/ml F-S Con A in PBS-BSA, then rinsed and mounted. Mitotic cells were identified in metaphase or early anaphase using phase-contrast optics on a modified Leitz microscope. The distribution of surface label on individual cells was then followed as a function of time at room temperature or at 37°C with a series of high-resolution multipoint fluorescence scans. These scans were generated by first focusing an attenuated laser beam from an argon-ion laser ($\lambda = 488$ nm) through the incident-light illuminator of the microscope to a small spot on the cell, and then moving the focused beam along a linear axis by a galvanometric scanning mirror. In cells undergoing cytokinesis, this axis ran perpendicular to the cleavage furrow through the poles. $F(x, t)$, the fluorescence intensity as a function of position along the scan axis, was detected by a thermoelectrically cooled photomultiplier tube, and quantified with photon-counting electronics synchronized to the position of the scanning laser beam. The optical apparatus and electronics are described in more detail in a previous publication (17).

Two basic types of laser measurements are reported here. In the first, we did not perturb the system. The redistribution of surface label was followed through anaphase and telophase, with the laser scan aligned along the polar axis of the cell, perpendicular to the equatorial plane of the metaphase plate. In the second type, the fluorescence distribution was initially changed, in a controlled way, by

fluorescence photobleaching. Intense localized laser pulses were used to deplete the concentration of fluorescent molecules over one pole of the cell. Translational diffusion coefficients were estimated from the rate of redistribution of fluorophore back into the bleached region (17). This approach is known as fluorescence redistribution after photobleaching (FRAP).

In many of these experiments, scans were taken with the laser beam defocused with a cylindrical lens to a line along an axis in the sample plane perpendicular to the scan axis. In this configuration, the laser beam effectively integrates over the entire surface of the cell at each position x , removing variations in intensity due to edge effects and differences in cell width along the pole-pole axis. This modification eliminates possible ambiguity introduced by changes of cell shape during the later stages of cytokinesis (see Appendix B).

Electron Microscopy

Monolayers of J774.2 cells were labeled with biotinyl Con A-avidin peroxidase

and were processed for electron microscopy as described before (29). Thin sections were stained with uranyl acetate and lead for observation of general morphology. Unstained sections were examined for the distribution of surface bound lectin.

RESULTS

Video-Fluorescence Analysis of F-S Con A-Receptor Movement

The receptor redistribution that occurs during cytokinesis is shown for a single F-S Con A-labeled cell in Fig. 1. The cell was identified in metaphase from the chromosome pattern revealed by Hoechst 33662 fluorescence. At this point in the mitotic cycle, F-S Con A was distributed over the whole cell

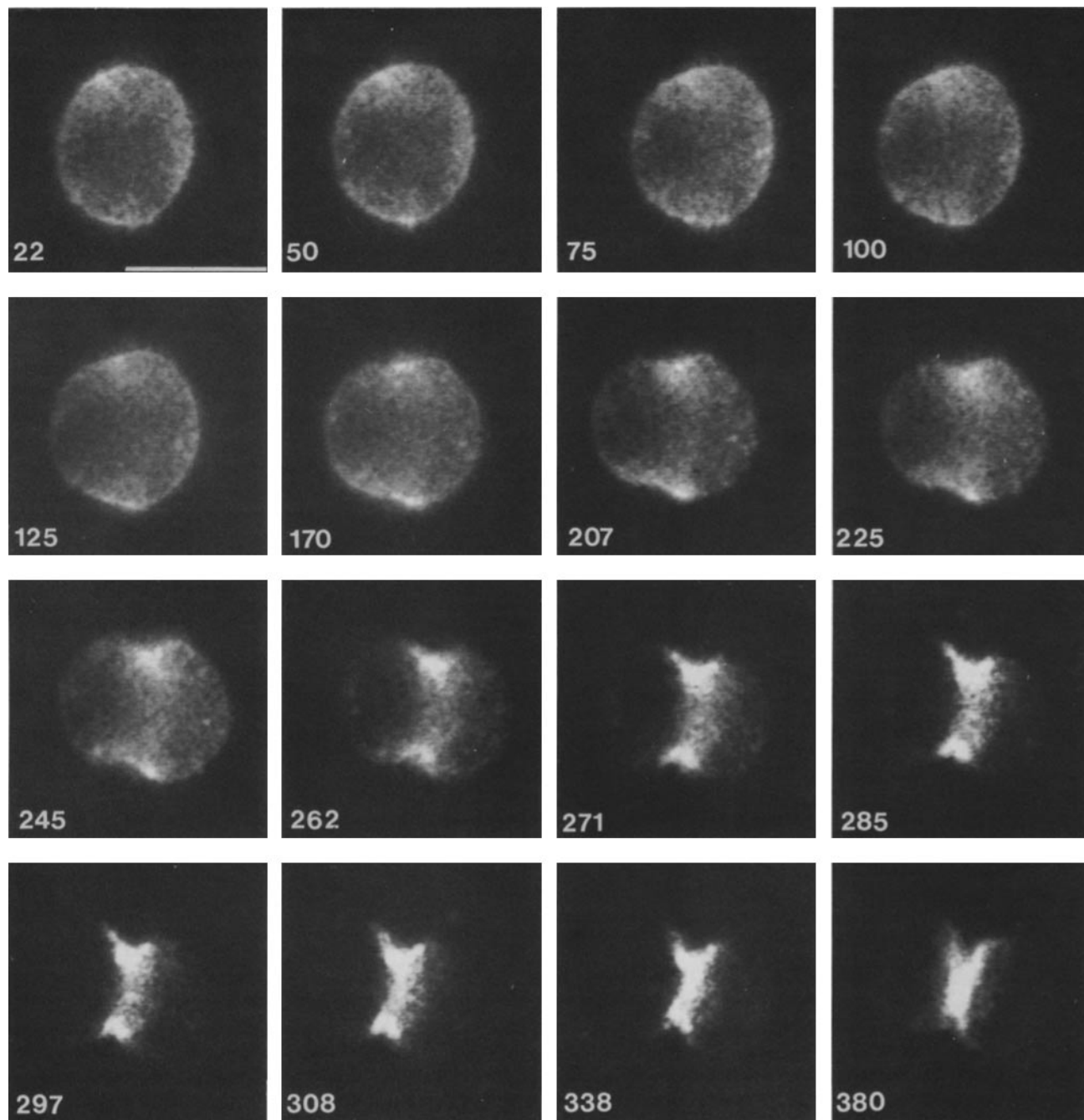


FIGURE 1 Frames from a video recording of a J774.2 macrophage labeled for 1 min at 37°C with F-S Con A, rinsed, mounted in culture medium on the 32°C stage of a Zeiss Universal microscope and viewed through an image intensification TV camera. Time is given in seconds. Bar, 20 μ m.

surface. However, the fluorescence redistributed into a belt encircling the cell body within a period of only 3 min (75–250 s on the time scale displayed on Fig. 1) at 32°C. This movement coincided with the appearance of the cleavage furrow. Indeed, it may precede it: at 50 s there appears to be a slight intensification of fluorescence over the area that will become the cleavage furrow before deformation of the membrane is detectable. This particular cell was observed over a subsequent 40-min period to confirm its apparently normal progression into G₁, with separation and migration of daughter cells.

We emphasize that most of the accumulation is complete by 270 s, by which time the cell has changed in shape only quite

modestly from an approximate sphere of 20- μ m diameter to a 23 μ m long belted cylinder. More pronounced cell shape change occurs as the cleavage furrow deepens: the apparent further increase in fluorescence intensity at the furrow as the daughter cells round up during this later period is probably due in part to the changing cell shape as one “looks down” the walls of the furrow.

Distribution of Membrane Folds during Cytokinesis

One trivial explanation for the redistribution of fluorescence

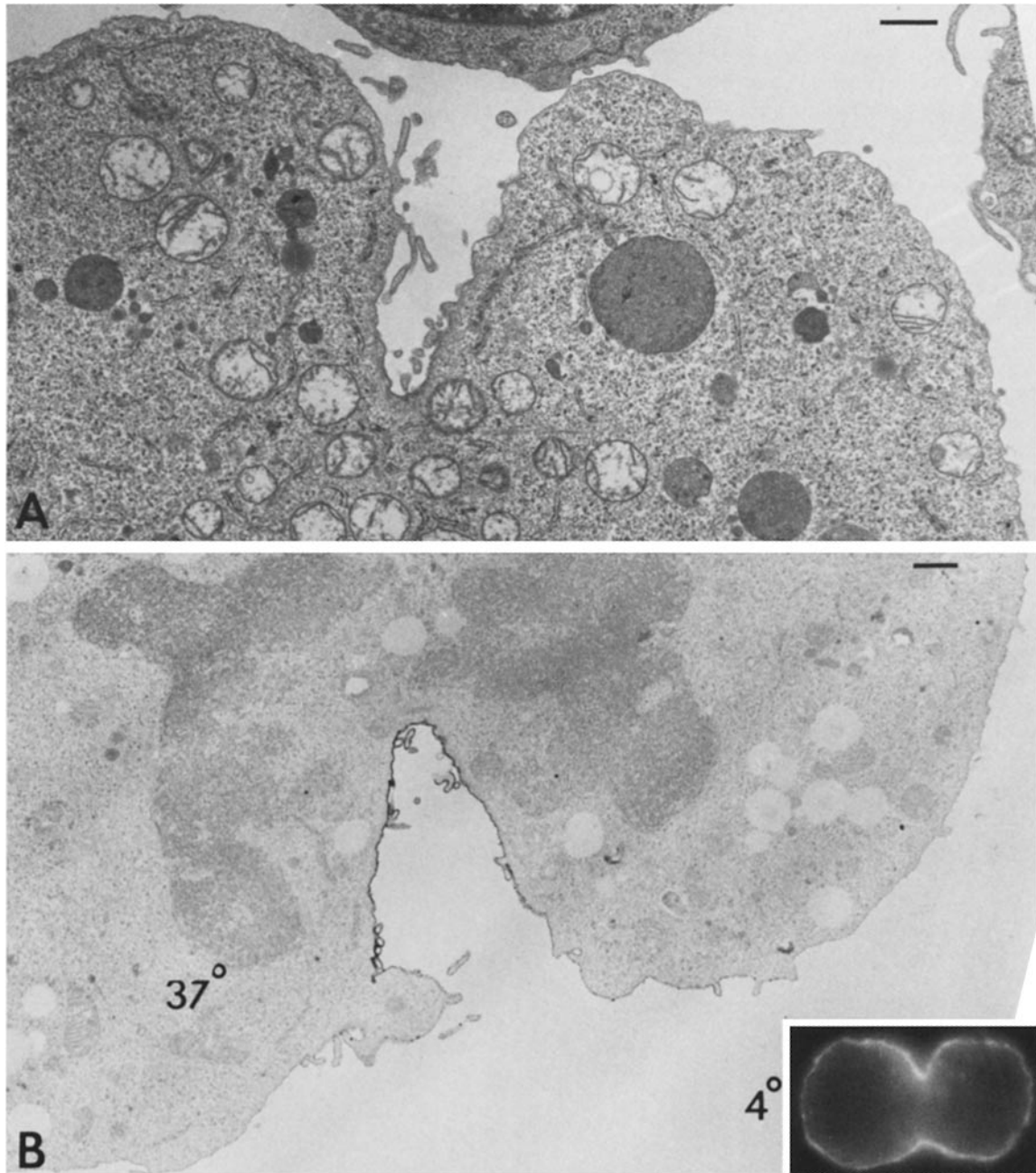


FIGURE 2 Morphology and surface distribution of Con A on dividing J774.2 macrophages. The stained thin section (A) shows the typical smooth poles and irregularly folded cleavage furrow of a cell in telophase. The unstained thin section (B) provides a similar view of a cell with surface label due to biotinyl Con A-avidin peroxidase (37°C label; 5 min). Lectin is cleared from the poles and accumulated at the furrow in this telophase cell. Bar, 1 μ m. The inset in B shows the relatively uniform distribution of fluorescence on a cell in late anaphase following binding of F-S Con A (100 μ g/ml) at 4°C for 5 min.

due to F-S Con A-receptor complexes during the early stages of cytokinesis is an artifact due to the accumulation of excess membrane and not the translocation of complexes at the cleavage furrow. We have marshalled evidence that suggests a minor increase in membrane folding at the cleavage furrow but which eliminates this phenomenon as a major cause of Con A-receptor accumulation. First, anaphase or telophase cells cooled then labeled at 4°C rather than 37°C with F-S Con A show only a hint of accumulation at the furrow (Fig. 2B, inset). Hence the majority of this receptor redistribution is ligand-induced. Second, thin-section electron microscopy shows only limited, and certainly not massive, folding of membrane at the cleavage furrow of dividing J774.2 macrophages (Fig. 2A). Third, thin sections of biotinyl Con A-avidin peroxidase-labeled cells reveal that lectin is indeed confined to the furrow and is removed from the poles of cells after incubation at 37°C for 5 min (Fig. 2B). Fourth, we have identified a fluorescent surface label that distributes uniformly in the membrane of J774.2 macrophages. The binding of a fluorescein conjugate of the B subunit of cholera toxin (F-CTB) to J774.2 macrophages is saturable and inhibitable by medium ganglioside, indicating a GM1 ganglioside receptor (7, 12). F-CTB appears to provide an intense, uniform label to even the most delicate membrane processes or folds on interphase cells (Fig. 3A). The same remarkably uniform distribution of F-CTB is also characteristic of cells in early anaphase (Fig. 3B). Most importantly cells at late anaphase (Fig. 3C) show F-CTB distributed uniformly over the whole surface, with only a hint of increased intensity at the furrow. This essentially uniform distribution on dividing cells was seen in the presence or absence of (unlabeled) succinyl Con A and on cells labeled at 4°C, 37°C without fixation, or after fixation in 4% paraformaldehyde.

Laser-Fluorescence Analysis of F-S Con A-Receptor Movement

The distribution of F-S Con A was quantified by photon counting during repetitive laser scans across cells as they progressed from metaphase to anaphase. The data were analyzed in terms of two simple alternative models of lateral movement (see Appendix A). In the first (the flow model), it is assumed that the net accumulation at the region of the developing cleavage furrow results from a directional flow of constant velocity, v , over the surface from the poles of the cell

(assumed to be a sphere of radius r) to the center. Random diffusion is taken to have a negligible effect. At the other extreme, the diffusion model assumes that molecular motion occurs only by random diffusion on the surface of the sphere with diffusion coefficient, D . In this case, we propose that surface complexes that diffuse to the center are immobilized and trapped, resulting in the observed accumulation.

The analysis proceeded in two stages. We first determined the effective values of v and D which, according to our model calculations, best fit the rates of fluorescence redistribution. This was accomplished by evaluating the decrease with time of the mean-squared widths of the fluorescence distributions. Photobleaching experiments were then performed on labeled mitotic cells to help distinguish between the two alternative modes of transport. Each of these approaches is discussed in turn below.

Mean-squared Width Analysis

Appendix A presents theoretical expressions derived for $c(x, t)$, the concentrations of label as functions of distance along the pole to pole axis, at time t after the initiation of redistribution. Experiments measure $F(x, t)$, the fluorescence intensity excited by a focused laser beam centered at position x along a linear scan axis. To facilitate the comparison between theory and experiment, we characterized each fluorescence scan by $\mu_2(t)$, its mean-squared width, or second moment about the mean along the scan axis (See Appendix B), calculated as

$$\mu_2(t) = \frac{\sum_i x_i^2 F(x_i, t)}{\sum_i F(x_i, t)} - \left[\frac{\sum_i x_i F(x_i, t)}{\sum_i F(x_i, t)} \right]^2 \quad (1)$$

The use of this particular parameter has several distinct advantages: (a) $\mu_2(t)$ can be calculated simply and objectively, according to Eq. 1, independent of transport model. It is not necessary to specify the area of label accumulation, or even indicate the positions of the cell boundaries. (b) The mean-squared width of $F(x, t)$ or $c(x, t)$ is expected to be especially sensitive to the extent of label depletion at the cell periphery, and relatively insensitive to the exact distribution of label accumulation at the cleavage furrow. Thus we are free to assume, in the model calculations, that the label accumulates as a simple delta function (see Appendix A). (c) A simple relationship exists between the mean-squared widths of $c(x, t)$

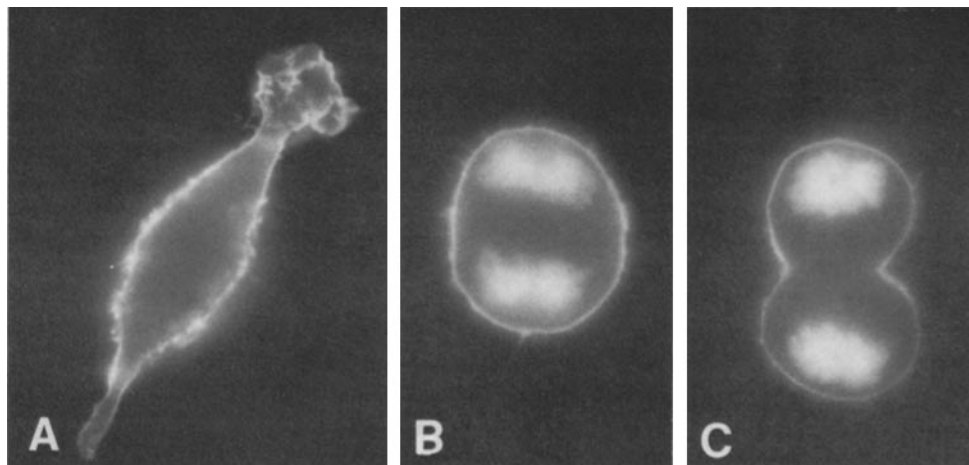


FIGURE 3 Distribution of F-CTB on J774.2 macrophages. Cell monolayers were incubated at 37°C for 10 min with F-CTB, then fixed with 4% paraformaldehyde and incubated with Hoechst 33258 to identify mitotic cells. The fluorescent ligand outlines the most delicate membrane folds and ruffles of the interphase cell (A). The regions of increased intensity most likely indicate regions of increased membrane accumulation. In contrast, a remarkably uniform

distribution of F-CTB fluorescence is seen at early anaphase before formation of the cleavage furrow (B). This essentially uniform labeling persists at late anaphase with only a hint of increased fluorescence intensity at the cleavage furrow (C). $\times 1,000$.

and $F(x, t)$ if fluorescence scans are taken with the laser beam defocused with a cylindrical lens to a line along an axis in the sample plane perpendicular to the scan axis. In this configuration, the laser beam effectively irradiates equal areas of membrane at each point of measurement eliminating the geometrical "edge effect" for the fluorescence intensity from the surface of a sphere. Under this condition, the mean-squared widths of $c(x, t)$ and $F(x, t)$ are expected to differ by only an additive constant (See Appendix B).

This property has two simple corollaries which open the way for two straight-forward strategies of analysis. Both R_{\max} , the maximum rate of change of $\mu_2(t)$, and $\tau^{1/2}$, the time corresponding to the midpoint in the total change, are clearly the same for $c(x, t)$ and $F(x, t)$. Effective values of v and D can thus be determined from the experimental values of R_{\max} and $\tau^{1/2}$ determined from the fluorescence data.

Fig. 4 presents theoretical plots of $\mu_2(t)$ for both transport models, along with an insert of the characteristic forms of $c(x, t)$ (See Appendix A).

For the flow model of redistribution, we have from Eq. B3:

$$R_{\max} = -(2/3)v r \quad (2a)$$

$$\tau^{1/2} = 0.30 r/v \quad (2b)$$

for the diffusion model of redistribution, solving Eq. B5 graphically:

$$R_{\max} = -0.47 D \quad (3a)$$

$$\tau^{1/2} = 0.40 r^2/D. \quad (3b)$$

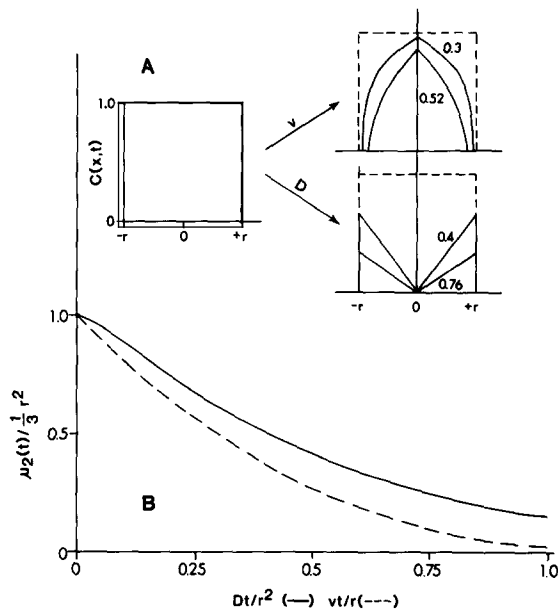


FIGURE 4 (A) Characteristic concentration distributions associated with the two transport models at time-zero (left) and at various times during the movement into the cleavage furrow for flow (upper right) and diffusion (lower right) (See Appendix A). The central vertical line indicates the site at which molecules are immobilized and accumulated. The numbers associated with each set of curves correspond to the values of the dimensionless times, vt/r (for flow) and Dt/r^2 (for diffusion) at which $\mu_2(t)/(1/3)r^2$ equals 0.5 and 0.25. (B) Theoretical values of $\mu_2(t)/(1/3)r^2$ for the concentration distributions calculated for the diffusion model (solid line) as a function of Dt/r^2 , and the flow model (dashed line) as a function of vt/r (See Appendix B).

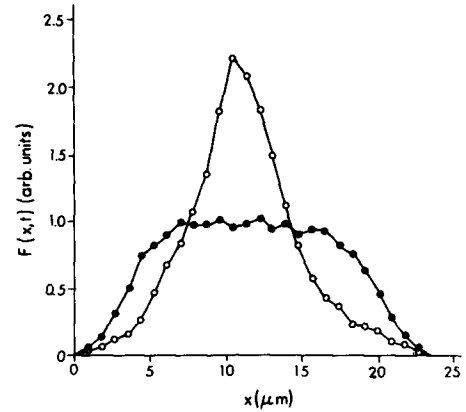


FIGURE 5 Typical scans of F-S Con A fluorescence on a mitotic J774 macrophage in early anaphase (●), and 7 min later in telophase (○). To reduce the ambiguity introduced by the changing membrane geometry, the scans were taken with the laser beam focused to a narrow line on the sample perpendicular to the scan axis. $T = 37^\circ C$.

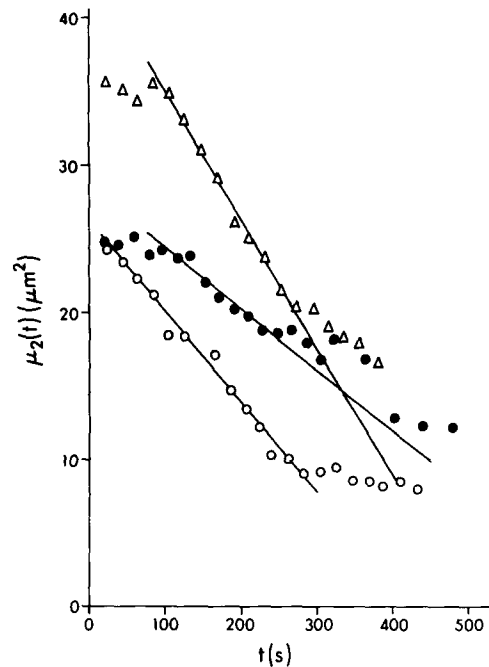


FIGURE 6 Time course of calculated $\mu_2(t)$ for the distribution of F-S Con A fluorescence on three J774 macrophages followed through late anaphase and telophase. Slopes of straight lines superimposed on data were used in estimation of R_{\max} values. $T = 37^\circ C$.

Effective values of v and D can thus be determined from the experimental values of R_{\max} and $\tau^{1/2}$ determined from the fluorescence data.

Fig. 5 shows two laser fluorescence scans on the same F-S Con A labeled macrophage in early anaphase (●), before detectable accumulation, and 7 min later (○), in telophase, where there is a clear central accumulation. Over this period of time, the characteristic value of $\mu_2(t)$ for this cell decreased from $\sim 25 \mu m^2$ to around $12 \mu m^2$. Fig. 6 presents the complete time course of $\mu_2(t)$ of three labeled cells followed through later anaphase and telophase. Effective values of v and D were calculated for each set of data by the methods described (See Eqs. 2-3) above. The results of these calculations are summarized in Table I. As one might expect, the transport parameters derived from $\tau^{1/2}$ are consistently higher than those derived from R_{\max} . This follows if one considers that not all labeled

receptors are necessarily redistributed, as the models assume. The parameters determined from values of R_{max} (but not $\tau^{1/2}$) are averages over the mobile and immobile components.

Fluorescence Redistribution after Photobleaching

Although the mean-squared width analysis described above gives reliable effective values of v and D , it cannot by itself distinguish between the two alternative models. The two functional forms of $\mu_2(t)$ plotted in Fig. 4 are much too similar to provide the basis of such a determination. To help resolve the question we performed two types of FRAP experiments.

In the first set of experiments, we used the normal-mode analysis of diffusion on a spherical surface (18) to estimate the diffusion coefficient on metaphase cells, without the complicating effects of receptor accumulation. We obtained an average value of $\sim 1 \times 10^{-10}$ cm²/s, which is approximately an order of magnitude lower than the values of D theoretically required to account for the rate of receptor accumulation during anaphase and telophase (see Table I) by a diffusion process. This slow diffusion rate is probably not an artifact of dye-mediated photodamage accompanying the photobleaching. Supplementing earlier control experiments (16, 30, 31), it has recently been demonstrated that photobleaching of intact erythrocytes under aerobic conditions does not alter the lateral diffusion characteristics of the integral membrane protein band 3 (19). Because of the similarities of the erythrocyte plasma membrane to others, it is expected that the FRAP technique can provide a valid measurement of the lateral mobility of plasma membrane components in other intact cells.

These initial calculations of D by FRAP were made on metaphase cells as opposed to cells undergoing cleavage. It seemed possible that D could be increased dramatically during the transition from metaphase to anaphase. To approach this question, we bleached the fluorescent label at one pole of a cell in early anaphase, and monitored for evidence of diffusion back into the bleached area during the actual progress of late anaphase and telophase. One example of such an experiment is presented in Figs. 7 and 8. For these data, the fluorescence scans were taken with the monitoring laser beam focused to a circularly symmetric spot to emphasize the cell edges.

The fluorescence scan in Fig. 7A shows a relatively uniform concentration distribution before photobleaching, with little evidence of accumulation as yet. A localized photobleaching pulse was then used to decrease the concentration of intact fluorophore at one pole of the cell (the left side in Figs. 7 and 8) to 50% of its initial level (Fig. 7B). To bleach as uniformly as possible across the pole of the cell, the bleaching beam was defocused to a band perpendicular to the scan axis. The

fluorescence distribution along the scan axis immediately after bleaching, normalized by $F(x, -)$, a prebleach scan, is presented in an insert to Fig. 7B.

During the first few minutes after photobleaching, the usual rapid transition to a marked central accumulation (Fig. 7C) was observed. The key question is what happens at the bleached edge during the transition period? If accumulation at the developing cleavage furrow proceeded by a rapid diffusion process, then we should also have expected to see an initial redistribution back into the bleached area at a comparable rate. Systematic flow, on the other hand, would have led only to a further decrease in intensity at the bleached pole. Fig. 8, which shows the intensity with time at the center (furrow) and left and right edges, demonstrates that, in fact, there is no observable fluorescence recovery, i.e., back-diffusion at the bleached left edge.

Theoretical expressions used for the quantitative analysis of these data are presented in Appendix C. It is assumed that the fluorescence label on the cell is bleached uniformly within a cap (11, 22). We have then three floating parameters: z_0 , the

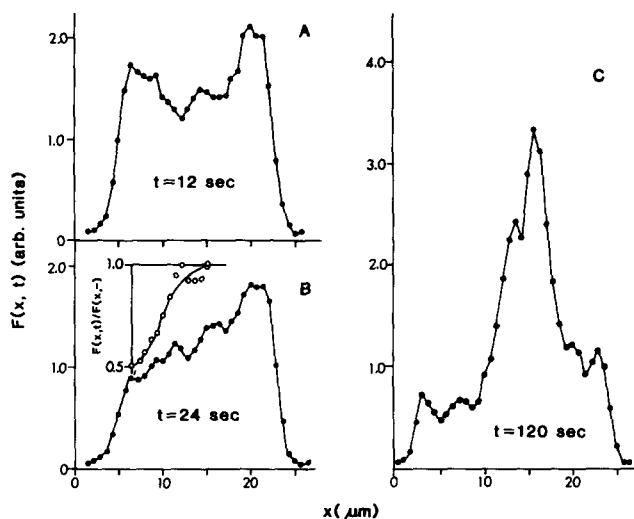


FIGURE 7 Scans of F-S Con A fluorescence on a mitotic J774 macrophage in late anaphase before photobleaching (A) immediately after a photobleaching laser pulse directed at edge of scan profile (B), and subsequently in telophase (C). Fluorescence scans were taken with the laser beam focused to a circularly symmetric spot, emphasizing the fluorescence at the cell edges and cleavage furrow. Bleaching was effected with a high intensity laser beam defocused to a band across the cell, perpendicular to the scan axis. The insert to B shows the immediate postbleach fluorescence distribution normalized by a prebleach scan. Three other cells showed qualitatively similar patterns.

TABLE I
Effective Values of v and D

Data*	r μm	$-R_{max} \times 10^2 \ddagger$ $\mu\text{m}^2/\text{s}$	$D \times 10^9 \S$ cm^2/s	$v \parallel$ $\mu\text{m}/\text{min}$	$\tau^{1/2}$ s	$D \times 10^9 \parallel$ cm^2/s	v^{**} $\mu\text{m}/\text{min}$
○	8.1	6.2	1.3	0.7	150	1.7	1.0
●	8.1	4.2	0.9	0.5	140	1.9	1.0
△	9.9	8.8	1.9	0.8	120	3.3	1.5
Avg \pm SD	—	—	1.4 ± 0.5	0.7 ± 0.2	—	2.3 ± 0.9	1.2 ± 0.3

* Symbols refer to data in Fig. 6.

‡ Corresponding to the slopes of the straight lines superimposed on data in Fig. 6.

§ Calculated from R_{max} using Eq. 3 a.

|| Calculated from R_{max} using Eq. 2 a.

¶ Calculated from $\tau^{1/2}$ using Eq. 3 b.

** Calculated from $\tau^{1/2}$ using Eq. 2 b.

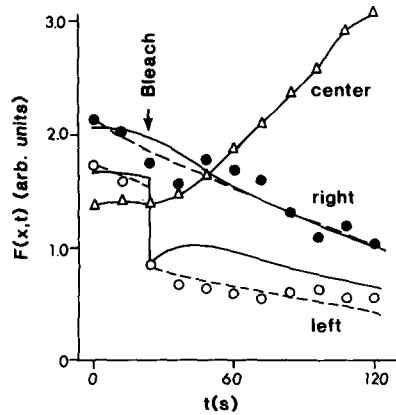


FIGURE 8 Time course of fluorescence intensity changes measured at the edges and site of central accumulation on the cell of Fig. 7. Each value is the average of three or four adjacent data points from a complete high-resolution fluorescence scan. The solid and dashed lines associated with the fluorescence data from the right (unbleached) and left

(bleached) edges of the cell are theoretical curves (See Appendix C) derived from the diffusion and flow models, respectively (see text).

cosine of equatorial angle at the cap boundary ($z_0 \leq \cos \theta \leq 1$ within the cap); α the fraction of fluorophore concentration left within the cap after bleaching; and D or v . In the present case, z_0 and α are estimated from the insert to Fig. 7B to be 0.6 and 0.5, respectively. Effective values of D and v are obtained by fitting the theoretical expressions to the time course of fluorophore concentration at the unbleached edge which thus acts as an internal control. A comparison is then made between the observed fluorescence intensity at the bleached edge, and the theoretical predictions, for the two modes of transport. The results are shown in Fig. 8. The solid lines for the "right" and "left" poles of the cell correspond to a diffusive transport with $D = 2.4 \times 10^{-9} \text{ cm}^2/\text{s}$. The dashed lines are for unidirectional flow with $v = 1.2 \text{ } \mu\text{m}/\text{min}$. It is seen that only the latter fits the observed behavior at the bleached left edge.

DISCUSSION

Two different procedures have been applied to observe and analyze the distribution of F-S Con A on the surface of dividing macrophages. One is based on video intensification image analysis and the other on laser scanning techniques. These procedures provide the first dynamic view of the remarkable redistribution of Con A-receptor complexes during cytokinesis. They confirm that the presence of F-S Con A does not inhibit progression of cells through the mitotic cycle. They show that the rapid movement of F-S Con A-receptor complexes occurs coincident with the appearance of the cleavage furrow. The video analysis is particularly valuable for its intuitive demonstration of the redistribution process and for the information it provides on cellular geometry as a function of F-S Con A redistribution. The laser analysis on the other hand has yielded quantitative data essential to distinguish flow from diffusional models of receptor redistribution.

Development of the quantitative analysis was predicated on the observed accumulation of ligand-receptor complexes representing a true redistribution in the membrane and not a purely geometrical effect. This consideration is not trivial. In general, the intensity across an image of cell-surface fluorescence is dependent upon both the concentration of label on the membrane and the geometry of the membrane. Simple geometrical considerations indicate that any cell capable of spreading out flat during interphase must necessarily contain an excess of plasma membrane when it rounds up during mitosis, i.e., an actual surface area much greater than the area of a

sphere of equal volume. It could thus be argued that the observed accumulation of receptor-ligand complexes might actually represent nothing more than an accumulation of excess whole membrane that simply accompanies the formation of the cleavage furrow.

The data, however, do not support this interpretation. First of all, the video fluorescence analyses (Fig. 1) illustrate that the bulk of F-S Con A redistribution is complete before the furrow is deeply invaginated and thus before optical effects are likely to present a serious problem of visual interpretation or quantitative analysis. In addition, the observed effect is ligand-induced. As shown in Fig. 2 (inset), significant accumulation of ligand-receptor complexes is observed only if the cells are incubated at room temperature or greater after ligand binding. Furthermore, thin section electron micrographs revealed very little accumulation of membrane at the cleavage furrow in J774.2 cells (Fig. 2A). We have also shown by thin section electron microscopy of Con A-peroxidase labeled cells that indeed the poles lack bound Con A under conditions where the furrow is heavily labeled (Fig. 2B). Finally we have shown that F-CTB provides a fluorescence probe for the most delicate membrane geometry in J774.2 cells. Using this probe, little or no evidence of excess membrane was detectable in the cleavage furrow in the presence or absence of succinyl Con A (Fig. 3). Interestingly we have also not found F-CTB or the complete fluorescein-labeled cholera toxin to be capped on J774 macrophages (R. D. Berlin and J. M. Oliver, unpublished observations). Since the B-fragment is probably present as a pentamer, some cross-linking of ganglioside GM₁ is probably present. The lack of accumulation of F-CTB in both the cleavage furrow and cell protuberance is consistent with the generally analogous behavior of these two structures. However, it is contrary to the earlier study of Craig and Cuatrecasas (7) who showed capping of the complete cholera toxin on lymphocytes. Aside from possible differences owing to cell type, the lymphocyte caps were formed over 30 min, a much longer period than required for accumulation in the cleavage furrow and resembled multiple aggregates on rounded cells rather than a single aggregate at a unique structural site.

With this information on cell shape and receptor distribution at hand, it was possible to proceed to the quantification of receptor redistribution which might, in turn, shed light on its mechanism.

As described above and further detailed in Appendices A and B, the laser fluorescence data were analyzed in terms of two models, one for receptor redistribution by a flow process and one by diffusion. The rate of receptor redistribution measured from our data is consistent with a characteristic flow velocity of $\sim 1 \text{ } \mu\text{m}/\text{min}$ or a diffusion coefficient of $\sim 10^{-9} \text{ cm}^2/\text{s}$, in the two alternative models of transport considered above.

A model for ligand-receptor movement based on diffusion and localized immobilization is not well supported by these data. The calculated required diffusion rate is an order of magnitude greater than diffusion coefficients measured by FRAP on metaphase cells ($10^{-10} \text{ cm}^2/\text{cm}$). This fact alone, however, cannot rule out a diffusion mechanism. Membrane protein diffusion rates are generally reduced to values very much smaller than that expected for free diffusion in membranes. For example, in normal mouse erythrocytes, the average diffusion coefficient of band 3 protein molecules is only 2% of that found in spectrin-deficient spherocytic erythrocytes, which lack the major component of the normal submembranous protein matrix (20, 27). It might thus be argued that Con

A receptor complexes could be freed of constraints and diffuse at the requisite rate during the period of movement to the furrow. This possibility is ruled out, however, by the data obtained after laser photobleaching presented in Figs. 7 and 8. Rapid diffusion would lead to an initial recovery of fluorescence at the bleached edge on the same time-scale as the accumulation at the developing cleavage furrow (Appendix C). This is not observed. Rather the redistribution of ligand-receptor is entirely towards the cleavage furrow. This clear demonstration of unidirectional movement seems to eliminate redistribution mechanisms that depend on the progressive cross-linking of receptors to achieve large aggregates of ligand-receptor complexes. Of course it does not eliminate as essential a smaller degree of diffusion-dependent cross-linking.

On the other hand, the anisotropy and the rate of accumulation of complexes in the cleavage furrow is readily compatible with a systematic flow model. According to the simple constant velocity model we present, flow rates of only $1 \mu\text{m}/\text{min}$ would be required for the directed movement of F-S Con A-receptor complexes during cell cleavage. We propose that this flow process is initiated coincident with the first appearance of the cleavage furrow. We predict that similar flow processes, perhaps involving the association of ligand-receptor complexes with membrane waves (see references 14, 24) may account for the characteristic redistribution of other membrane components and structures that accompany cytokinesis and analogous processes such as capping, phagocytosis, and chemotaxis.

APPENDIX A

MATHEMATICAL MODELS OF DIFFUSION AND FLOW: We consider again two models of transport leading to a net accumulation at the developing cleavage furrow: directional constant velocity flow on the cell surface from the cell poles to the center; and net diffusional flux caused by molecules sticking at the center. In both cases, for simplicity, we make the following assumptions: (a) The membrane contour of the cell is a spherical shell of radius r . This is a good representation during the early stages of mitosis, but is less satisfactory later on. (b) The concentration of label is uniform initially, and accumulates as an essentially infinitely narrow ring at the cleavage furrow (equatorial angle $\pi/2$), represented mathematically by a Dirac delta function. (c) All labeled molecules move at velocity v along arcs of constant azimuthal angle towards the cleavage furrow (flow model), or diffuse with diffusion coefficient D (diffusion model), up to the point of immobilization and accumulation.

In both models, the proposed modes of transport do not disrupt the initial azimuthal symmetry of the concentration distribution. Hence, the concentration distributions at time t , $c(z, t)$, are functions only of z , the cosine of equatorial angle θ .

Each model is fully characterized by a single parameter: the transport rate v/r (for the flow model), or D/r^2 (for the diffusion model). In the sections below, results are expressed in terms of normalized, dimensionless times, defined as

$$t_v = vt/r \quad (\text{A1a})$$

$$t_D = Dt/r^2. \quad (\text{A1b})$$

FLOW MODEL: The solution for the concentration distribution can be written directly. Considering one of the hemispheres ($0 \leq \theta \leq \pi/2$), the flow completely removes the labeled complexes from the cap defined by $0 \leq \theta \leq t_v$. At the same

time, the concentration decreases in the region $t_v < \theta < \pi/2$ because of a geometrical effect analogous to the familiar radial dilution in a sector-shaped ultracentrifuge cell. We thus have (excluding the delta function term at $\theta = \pi/2$):

$$c(\theta, t_v) = \frac{\sin(\theta - t_v)}{\sin \theta} \quad \text{if} \quad \left(t_v < \theta < \frac{\pi}{2} \right) \quad (\text{A2})$$

$$= 0 \quad \text{if} \quad (0 \leq \theta < t_v)$$

or, for $0 < z < \cos t_v$,

$$c(z, t_v) = \cos t_v - (\sin t_v)z(1 - z^2)^{-1/2}. \quad (\text{A3})$$

$c(z, t_v)$ on the other hemisphere would simply be the mirror image about $z = 0$. Fig. 4A presents representative graphs of $c(z, t_v)$ for different values of t_v .

DIFFUSION MODEL: For free diffusion on the surface of a sphere, the general solution of the diffusion equation has the form (15):

$$c(z, t_D) = \sum_{n=0}^{\infty} A_n P_n(z) \exp[-n(n+1)t_D], \quad (\text{A4})$$

where $P_n(z)$ is the n th Legendre polynomial, and, since the Legendre polynomials are orthogonal,

$$A_n = \frac{2n+1}{2} \int_{-1}^1 c(z, 0) P_n(z) dz. \quad (\text{A5})$$

We seek a specific solution (a specific set of A_n 's) consistent with the following boundary conditions: (i) $c(z, t_D) = 1$ for $t_D < 0$ (where $t_D = 0$ defines the initiation of redistribution); (ii) $c(z, t_D) = 0$ at $z = 0$ for all $t_D \geq 0$. This latter condition establishes the equatorial ring at $z = 0$ as a "sink" of diffusing complexes (reference 8; complexes immobilized at $z = 0$ no longer exist as far as the diffusion equation is concerned).

Both boundary conditions can be satisfied for the consideration of the concentration on one hemisphere ($0 \leq z \leq 1$) if we choose the following effective initial distribution over the entire sphere:

$$c(z, 0) = \begin{matrix} 1 & \text{if} & (0 < z \leq 1) \\ 0 & \text{if} & (z = 0) \\ -1 & \text{if} & (-1 \leq z < 0). \end{matrix} \quad (\text{A6})$$

Diffusion does not disrupt the initial overall symmetry established by the negative concentration on the other hemisphere, maintaining $c(z, t_D) = 0$ at $z = 0$ for all subsequent times. Plugging Eq. A6 back into Eq. A5 gives

$$A_n = (2n+1) \int_0^1 P_n(x) dx \quad (\text{for } n \text{ odd}) \quad (\text{A7})$$

$$= 0 \quad (\text{for } n \text{ even})$$

or, applying standard recurrence relationships for the Legendre polynomials (Eqs. 25.23 and 25.20 of reference 28),

$$A_n = \frac{2n+1}{n+1} P_{n-1}(0) \quad (n \text{ odd}). \quad (\text{A8})$$

Representative graphs of $c(z, t_D)$, calculated from Eqs. A4 and A8 for $0 \leq z \leq 1$, and drawn as the mirror image for $-1 \leq z \leq 0$, are presented in Fig. 4A.

APPENDIX B

MOMENTS AND CUMULANTS OF THE CONCENTRATION

AND FLUORESCENCE DISTRIBUTIONS: The second moments of the concentration distributions about $z = 0$ (i.e., the second cumulants, or mean squared widths) can be determined for the results derived in Appendix A. In general, for a symmetric distribution

$$\mu_2(t) = 2r^2 \int_0^1 z^2 c(z, t) dz / \int_{-1}^1 c(z, t) dz. \quad (\text{B1})$$

The immobile complexes accumulated as a delta function at $z = 0$ do not contribute to the numerator of Eq. B1, but are included in the denominator so that

$$1/2 \int_{-1}^1 c(z, t) dz = 1, \quad (\text{B2})$$

by conservation of mass, for all times.

For the flow model, substituting Eq. A3 into Eq. B1, we obtain

$$\mu_2(t_D) = (r^2/3)(1 - \sin t_D)^2. \quad (\text{B3})$$

Likewise, substituting Eqs. A4 and A8 for the diffusion model into Eq. B1, we get

$$\mu_2(t_D) = r^2 \sum_{n \text{ odd}} \frac{2n+1}{n+1} P_{n-1}(0) \cdot \exp[-n(n+1)t_D] \int_0^1 z^2 P_n(z) dz. \quad (\text{B4})$$

Integrating by parts two times, applying two recurrence formulii for the Legendre polynomials (Eqs. 25.23 and 25.20, Ref. 28), gives finally,

$$\mu_2(t_D) = 2r^2 \sum_{n \text{ odd}} \frac{2n+1}{(2-n)n^2(n+3)} \cdot [P_{n+1}(0)]^2 \exp[-n(n+1)t_D]. \quad (\text{B5})$$

Calculated values of $\mu_2(t)$, calculated according to Eqs. B3 and B5, are presented in Fig. 4B.

In laser scan experiments, we measure $F(x, t)$, the fluorescence intensity excited by a focused laser beam centered at position x along the scan axis. We can demonstrate, however, that under appropriate conditions the second moments about the mean of $F(x, t)$ and $c(x, t)$ differ by only an additive constant. When this relationship holds, the expressions derived for R_{\max} and $\tau_{1/2}$ for the model calculations of $c(x, t)$ can be used to analyze the moments of the fluorescence data directly.

In general, to good approximation,

$$F(x, t) = \int_{-\infty}^{\infty} \int_{-\infty}^{\infty} c(x', y', t) I(x - x', y') s(x', y') dx' dy' \quad (\text{B6})$$

where $I(x', y')$ is the intensity profile of the laser beam focused onto the cell midplane, and $s(x', y') dx' dy'$ is the membrane surface area at position x', y' within increment $dx' dy'$. Eq. B6 simplifies considerably under the following conditions: (i) The concentration of surface label is constant across the width of the cell perpendicular to the scan axis; i.e., $c(x', y', t)$ is independent of y' , as we have assumed. (ii) The laser beam is defocused perpendicular to the scan axis to a line very much longer than it is wide; i.e., $I(x', y')$ can be taken as independent

of y' . (iii) $[\int_{-\infty}^{\infty} s(x', y') dy'] dx'$, the membrane surface area across the cell at position x' within increment dx' is constant along the entire scan axis. This condition is obviously valid for the trivial case of a planar membrane, or for a cylindrical shell of membrane oriented along the scan axis. It also holds for the more realistic geometry of a spherical shell, or two fused spherical shells. Incorporating these conditions into Eq. B6, we then have

$$F(x, t) = \int_{-\infty}^{\infty} c(x', t) I(x - x') dx'; \quad (\text{B7})$$

i.e., $F(x, t)$ is simply equal to the convolution of $c(x, t)$ with $I(x)$.

Since variance is an additive under convolution (4), the second moment of the measured $F(x, t)$ differs from the second moment of the actual concentration of fluorophore by only the second moment of the laser profile on the surface, which is the additive constant of our original thesis. This additive relationship holds, in general, for the cumulants of the distributions of any order m . The variance is the special case for $m = 2$.

APPENDIX C

FLUORESCENCE REDISTRIBUTION AFTER PHOTO-BLEACHING: It is assumed that one pole of the cell ($z_0 < z \leq 1$), is uniformly bleached initially to a fraction, α , of its initial level (11, 22). In practice, this condition is approximated by sweeping a bleaching beam, defocused in one dimension to a line perpendicular to the scan axis, onto the pole. From subsequent fluorescence scans with a monitoring beam, we estimate

$$f(t) = \frac{1}{1 - z_0} \int_{z_0}^1 c(z, t) dz, \quad (\text{C1})$$

the average concentration of label within the bleached pole, as a function of time after the initiation of label accumulation at $z = 0$.

In the flow model of accumulation $f(t)$ decreases monotonically, and is simply proportional to the values that would be observed in the absence of bleaching. Thus, combining Eqs. A3 and C1,

$$f(t_D) = \alpha \frac{1 - \cos(\cos^{-1} z_0 - t_D)}{1 - z_0}. \quad (\text{C2})$$

In the diffusion model, $f(t)$ increases initially, as labeled complexes diffuse back into the bleached region. We need a new solution of the diffusion equation for the initial condition.

$$\begin{aligned} c(z, 0) &= \alpha & \text{if } (z_0 < z \leq 1) \\ &= 1 & \text{if } (0 < z < z_0) \\ &= -1 & \text{if } (-z_0 < z < 0) \\ &= -\alpha & \text{if } (-1 \leq z < -z_0). \end{aligned} \quad (\text{C3})$$

Combining Eqs. A4, A5, C1, and C3, we have, in this case,

$$f(t_D) = \frac{1}{1 - z_0} \sum_{n \text{ odd}} (2n+1) [g_n(0) - (1 - \alpha) g_n(z_0)] g_n(z_0) \exp[-n(n+1)t_D], \quad (\text{C4})$$

where we have defined

$$g_n(z') = \int_{z'}^1 P_n(z) dz \quad (C5)$$

$$= \frac{1}{2n+1} [P_{n-1}(z') - P_{n+1}(z')].$$

We thank Mr. D. Goff for capable assistance with the laser fluorescence studies. We also thank Ms. J. R. Pfeiffer for preparation of the electron micrographs.

This work was supported in part by National Institutes of Health grants GM23585, CA15544, HL-23192, ES-01106 and grant BC179 from the American Cancer Society. Janet M. Oliver is also supported by a Faculty Research Award from the American Cancer Society.

Received for publication 8 June 1981, and in revised form 26 January 1982.

REFERENCES

- Berlin, R. D., and J. M. Oliver. 1978. Analogous ultrastructure and surface properties during capping and phagocytosis in leukocytes. *J. Cell Biol.* 77:789-804.
- Berlin, R. D., J. M. Oliver, and R. J. Walter. 1978. Surface functions during mitosis. I. Phagocytosis, pinocytosis and mobility of surface-bound Con A. *Cell.* 15:327-341.
- Berlin, R. D., and J. M. Oliver. 1980. Surface functions during mitosis. II. Quantitation of pinocytosis and kinetic characterization of the mitotic cycle using a new fluorescence technique. *J. Cell Biol.* 85:660-671.
- Bracewell, R. N. 1978. *The Fourier Transform and its Application*. McGraw-Hill, Inc., New York.
- Braun, J., K. Fujiwara, T. D. Pollard, and E. R. Unanue. 1978. Two distinct mechanisms for redistribution of lymphocyte surface macromolecules. I. Relationship to cytoplasmic myosin. *J. Cell Biol.* 79:409-418.
- Bretscher, M. S. 1976. Directed lipid flow in cell membranes. *Nature (Lond.)* 260: 21-23.
- Craig, S. W., and P. Cuatrecasas. 1975. Mobility of cholera toxin receptors on rat lymphocyte membranes. *Proc. Natl. Acad. Sci. U. S. A.* 72:3844-3848.
- Crank, J. 1956. *The Mathematics of Diffusion*. Oxford University Press.
- DePetris, S. 1977. Distribution and mobility of plasma membrane components on lymphocytes. In *Dynamic Aspects of Cell Surface Organization*. Ed. G. Poste and G. L. Nicolson, editors. Elsevier-North Holland, New York. 644-728.
- Edelman, G. M. 1976. Surface modulation in cell recognition and cell growth. *Science (Wash. D. C.)* 192: 218-226.
- Edidin, M., Y. Zagyansky, and T. J. Lardner. 1976. Measurements of membrane protein lateral diffusion in single cells. *Science (Wash. D. C.)* 191:466-468.
- Hansson, H.-A., J. Holmgren, and L. Swennerholm. 1977. Ultrastructural localization of cell membrane GM₁ ganglioside by cholera toxin. *Proc. Natl. Acad. Sci. U. S. A.* 74:3782-3786.
- Harris, A. K. 1976. Recycling of dissolved plasma membrane components as an explanation of the capping phenomenon. *Nature (Lond.)* 263:781-783.
- Hewitt, J. A. 1979. Surf-riding model for cell capping. *J. Theor. Biol.* 80:115-127.
- Huang, H. W. 1973. Mobility and diffusion in plane of cell membrane. *J. Theor. Biol.* 40:11-17.
- Jacobson, K., Y. Hou, and J. Wojcieszyn. 1978. Evidence for lack of damage during photobleaching measurements of the lateral mobility of cell surface components. *Exp. Cell Res.* 116:179-189.
- Koppel, D. E. 1979. Fluorescence redistribution after photobleaching. A new multipoint analysis of membrane translational dynamics. *Biophys. J.* 28:281-291.
- Koppel, D. E., M. P. Sheetz, and M. Schindler. 1980. Lateral diffusion in biological membranes. A normal-mode analysis of diffusion on a spherical surface. *Biophys. J.* 30:187-192.
- Koppel, D. E., and M. P. Sheetz. 1981. Fluorescence photobleaching does not alter the lateral mobility of erythrocyte membrane glycoprotein. *Nature (Lond.)* 293:159-161.
- Koppel, D. E., M. P. Sheetz, and M. Schindler. 1981. Matrix control of protein diffusion in biological membranes. *Proc. Natl. Acad. Sci. U. S. A.* 78:3576-3580.
- Kurosky, A., D. E. Markel, B. Touchstone, and J. W. Peterson. 1976. Chemical characterization of the structure of cholera toxin and its natural toxoid. *J. Infect. Dis.* 133:514-522.
- Lardner, T. J., and N. Solomon. 1976. The determination of local cell membrane diffusion coefficients. *J. Theor. Biol.* 60:433-440.
- Muschel, R. L., N. Rosen, and B. R. Bloom. 1977. Isolation of variants in phagocytosis of a macrophage-like continuous cell line. *J. Exp. Med.* 145:175-186.
- Oliver, J. M., and R. D. Berlin. 1982. Mechanisms that regulate the structural and functional architecture of cell surfaces. *Int. Rev. Cytol.* 74:55-94.
- Ralph, P., and I. Nakoinz. 1975. Phagocytosis and cytolysis by a macrophage tumor and its cloned cell line. *Nature (Lond.)* 257:393-394.
- Schreiner, G. F., and E. R. Unanue. 1976. Membrane and cytoplasmic changes in B lymphocytes induced by ligand-surface immunoglobulin interaction. *Adv. Immunol.* 24:38-165.
- Sheetz, M. P., M. Schindler, and D. E. Koppel. 1980. Lateral mobility of integral membrane proteins is increased in spherocytic erythrocytes. *Nature (Lond.)* 285:510-512.
- Spiegel, M. R. 1968. *Mathematical handbook of formulas and tables*. McGraw-Hill Book Co., New York.
- Walter, R. J., R. D. Berlin, J. R. Pfeiffer, and J. M. Oliver. 1980. The polarization of endocytosis and receptor topography on cultured macrophages. *J. Cell Biol.* 86:199-211.
- Wey, C.-L., R. A. Cone, and M. A. Edidin. 1981. Lateral diffusion of rhodopsin in photoreceptor cells measured by fluorescence photobleaching and recovery. *Biophys. J.* 33:225-232.
- Wolf, D. E., M. A. Edidin, and P. R. Dragsten. 1980. Effect of bleaching light on measurements of lateral diffusion in cell membranes by fluorescence photobleaching recovery method. *Proc. Natl. Acad. Sci. U. S. A.* 77:2043-2045.